

# Dilepton production in proton-proton and Pb+Pb collisions at $\sqrt{s_{\text{NN}}} = 2.76$ TeV

O. Linnyk\* and W. Cassing

*Institut für Theoretische Physik, Universität Giessen, 35392 Giessen, Germany*

J. Manninen and E. L. Bratkovskaya

*Institut für Theoretische Physik, Johann Wolfgang Goethe University, 60438 Frankfurt am Main, Germany; Frankfurt Institute for Advanced Studies, 60438 Frankfurt am Main, Germany;*

P. B. Gossiaux and J. Aichelin

*SUBATECH, UMR 6457, Laboratoire de Physique Subatomique et des Technologies Associées, University of Nantes - IN2P3/CNRS - Ecole des Mines de Nantes, 44072 Nantes Cedex 03, France;*

T. Song and C. M. Ko

*Cyclotron Institute and Department of Physics and Astronomy, Texas A&M University, College Station, TX 77843-3366, USA*

(Dated: August 8, 2012)

We study  $e^+e^-$  pair production in proton-proton and central Pb+Pb collisions at  $\sqrt{s_{\text{NN}}} = 2.76$  TeV within two models: an extended statistical hadronization model (SHM) and the Parton-Hadron-String Dynamics (PHSD) transport approach. We find that the PHSD calculations roughly agree with the dilepton spectrum from hadronic sources with the ‘cocktail’ estimates from the statistical hadronization model matched to available data at LHC energies. The dynamical simulations within the PHSD show a moderate increase of the low mass dilepton yield essentially due to the in-medium modification of the  $\rho$ -meson. Furthermore, pronounced traces of the partonic degrees of freedom are found in the PHSD results in the intermediate mass regime. The dilepton production from the strongly interacting quark-gluon plasma (sQGP) exceeds that from the semi-leptonic decays of open charm and bottom mesons. Additionally, we observe that a transverse momentum cut of 1 GeV/c further suppresses the relative contribution of the heavy meson decays to the dilepton yield, such that the sQGP radiation strongly dominates the spectrum for masses from 1 to 3 GeV, allowing a closer look at the electromagnetic emissivity of the partonic plasma in the early phase of Pb+Pb collisions.

PACS numbers: 25.75.-q, 13.60.Le, 14.40.Lb, 14.65.Dw

## I. INTRODUCTION

Dileptons, i.e. correlated electron and positron or  $\mu^+\mu^-$  pairs, are one of the key observables in experiments for ultra-relativistic nuclear collisions since they are emitted during the whole evolution of a collision and interact only electromagnetically and thus very weakly with the strongly interacting partonic or hadronic medium created in the collisions. Also, dileptons of different invariant masses are dominantly produced from different stages of a relativistic nuclear collision, and this provides the possibility to probe the properties of the produced hot and dense matter at various conditions by measuring the differential dilepton spectra.

The invariant mass spectrum of dileptons can be roughly divided into 3 different regions which are dominated by different physics. In the low mass region ( $M_{e^+e^-} < 1$  GeV), the radiation is dominated by the decays of light mesons (consisting of  $u$ ,  $d$  and  $s$  (anti)quarks), while in the intermediate mass region ( $1 \text{ GeV} < M_{e^+e^-} < 3 \text{ GeV}$ ), the dominant hadronic con-

tribution to the invariant mass spectrum stems from the decays of open charm mesons. Above the  $J/\psi$  peak, the dilepton spectrum is first dominated by open beauty decays and then by the initial state Drell-Yan radiation. Besides these sources of dileptons, the radiation from the strongly interacting Quark-Gluon-Plasma (sQGP) [1] as well as some other more exotic sources like simultaneous interactions of four pions [2–5] can also give significant contributions, particularly in the intermediate mass region. These partonic and hadronic channels have been studied in detail in Refs. [6, 7] at top Super-Proton-Synchrotron (SPS) and Relativistic-Heavy-Ion-Collider (RHIC) energies, and it has been found that the partonic channels clearly dominate over multi-pion sources in the intermediate dilepton mass regime.

In the present study, we include all known (leading) dilepton sources to study and compare the magnitude of the radiation from the QGP with that from other (conventional) sources in heavy ion collisions at the Large-Hadron-Collider (LHC) energies. Since at present there is no single model that could address reliably all of the above-mentioned sources for dilepton production, we thus employ in this analysis different approaches to evaluate the invariant mass spectrum from the different sources. Specifically, we concentrate on two models (and

---

\*Electronic address: Olena.Linnyk@theo.physik.uni-giessen.de

their extensions): The Parton-Hadron-String-Dynamics (PHSD) approach [8, 9] and the extended Statistical Hadronization Model (SHM) [10]. The PHSD model is a relativistic transport approach developed, tested and well suited for studying dynamical partonic and hadronic systems in heavy ion collisions from low to ultra-relativistic energies of  $\sqrt{s_{NN}}=200$  GeV, while the SHM is a statistical hadronic model suitable for describing in detail the relative yields of final state hadrons.

In the case of proton-proton ( $pp$ ) collisions, they are dominated by the creation and decays of various hadrons, and the SHM should be a suitable model for estimating the hadronic freeze-out 'cocktail' contribution to dileptons. Indeed, this was confirmed by our simulations in Ref. [10] for  $p+p$  collisions at  $\sqrt{s_{NN}}=200$  GeV. On the contrary, in heavy-ion collisions a rather long-living strongly interacting dynamical fireball is formed and dileptons are emitted from the created charges over an extended period of time. For such systems the SHM might not provide a good description because the properties, i.e. the masses and widths, of hadrons might change in the hot and dense nuclear environment as a function of time, which can not be taken into account in the SHM. Additionally, the dilepton signal from the QGP during the early reaction phase is expected to outshine the background radiation due to the cocktail of hadron decays. For this purpose, we will employ the PHSD transport approach which can account for the medium-dependent properties of partons and hadrons and their multiple interactions as well as for the dynamical evolution of the system in general, including the transition to the partonic phase and the radiation from the sQGP.

We note that a direct comparison between results from the PHSD and the SHM has shown that the low mass ( $M < 1$  GeV) spectra of  $e^+e^-$ -pairs in  $Au+Au$  collisions at  $\sqrt{s_{NN}}=200$  GeV deviate from each other by only up to 20% [7, 10], i.e. either the time-evolution of the system plays only a minor role in the dilepton emission or the subsequent hadronic evolution to a large extent washes out the details of the dynamics in the dilepton invariant mass spectrum. We will study this issue again in detail in the first part of present study and compare explicitly our results from both the static and dynamical model in order to constrain the dilepton yield from known hadronic sources. We will then proceed to our main goal, i.e. the identification of the QGP signal from the spectrum of dileptons produced in  $Pb+Pb$  collisions in the LHC energy regime.

In the following Section (Sect. II), we will briefly recall the main concepts of the PHSD transport approach and list the partonic and hadronic sources of dileptons in PHSD. Next, we describe the SHM and the way hadron yields and spectra are evaluated in Sect. III. Our treatment of  $D$  and  $B$  meson production and energy loss is described in Sect. IV, whereas the modeling of charmonia production in elementary and in nucleus-nucleus collisions is outlined in Sect. V. Results from our study are presented in Sect. VI. We first include a discussion of

dilepton production in the baseline  $p+p$  collisions. We then continue with results from the SHM as well as from the dynamical calculations of  $Pb+Pb$  collisions within the PHSD. Furthermore, the effect of in-medium modifications of vector mesons on the low-mass dilepton spectrum at  $\sqrt{s_{NN}}=2.76$  TeV is investigated. Finally, the influence of a transverse momentum cut on the dilepton spectrum as a possible way to enhance the QGP signal is explored. We conclude our study in Sect. VII with a summary of our findings and a discussion of open problems.

## II. THE PARTON-HADRON-STRING DYNAMICS (PHSD) TRANSPORT APPROACH

The PHSD model [8, 9] is an off-shell transport model that consistently describes the full evolution of a relativistic heavy-ion collision from the initial hard scatterings and string formation through the dynamical deconfinement phase transition to the quark-gluon plasma as well as hadronization and to the subsequent interactions in the hadronic phase. In the hadronic sector, the PHSD is equivalent to the Hadron-String-Dynamics (HSD) transport approach [11–13] that has been used for the description of  $pA$  and  $AA$  collisions from SIS to RHIC energies and has led to a fair reproduction of measured hadron abundances, rapidity distributions and transverse momentum spectra. In particular, as in the HSD, the PHSD incorporates off-shell dynamics for vector mesons [14] and a set of vector-meson spectral functions [15] that covers possible scenarios for their in-medium modifications. In PHSD the transition from the partonic to hadronic degrees of freedom is described by covariant transition rates for the fusion of quark-antiquark pairs to mesonic resonances or three quarks (antiquarks) to baryonic states, i.e., by the dynamical hadronization [16]. Note that due to the off-shell nature of both partons and hadrons, the hadronization process obeys all conservation laws (i.e., the 4-momentum conservation and the flavor current conservation) in each event, the detailed balance relations, and the increase in the total entropy  $S$ . The transport theoretical description of quarks and gluons in the PHSD is based on a Dynamical QuasiParticle Model (DQPM) for partons that is constructed to reproduce the lattice QCD (lQCD) results for a quark-gluon plasma in thermodynamic equilibrium. The DQPM provides the mean-fields for gluons/quarks and their effective 2-body interactions that are implemented in the PHSD. For details about the DQPM model and the off-shell transport, we refer the reader to the review in Ref. [17].

We stress that a non-vanishing width in the partonic spectral functions is the main difference between the DQPM and conventional quasiparticle models [18]. Its influence on the collision dynamics can be seen in the correlation functions, which, in the stationary limit involve the off-diagonal elements of the energy-momentum tensor  $T^{kl}$  and thus give rise to the shear viscosity  $\eta$  of

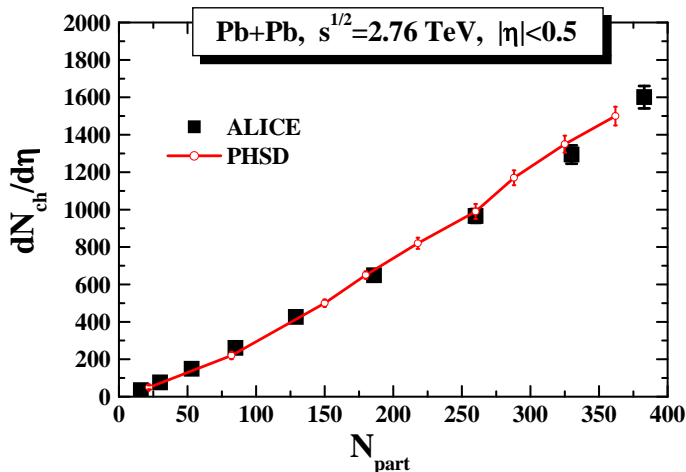


FIG. 1: (Color on-line) Pseudo-rapidity distribution of charged hadrons at midrapidity as a function of the number of participants  $N_{part}$  from PHSD (solid line) in comparison to the data from the ALICE Collaboration [23] for Pb+Pb at  $\sqrt{s_{NN}} = 2.76$  TeV.

the medium [19]. A sizable width is then essential for obtaining a small ratio of the shear viscosity to entropy density  $\eta/s$ , which results in a roughly hydrodynamical evolution of the partonic system in PHSD [16]. The two-particle correlations resulting from the finite width of the parton spectral functions are taken into account dynamically in the PHSD by means of the *generalized* off-shell transport equations [14] that go beyond the mean field or Boltzmann approximation [17, 20].

We recall that the PHSD approach has been tested from low SPS to top RHIC energies against the measured rapidity spectra of various particle species, transverse mass distributions, differential elliptic flow of charged hadrons as well as their quark-number scaling [21]. More recently, higher harmonics in the azimuthal distribution of charged hadrons in the plane perpendicular to the beam direction has also been examined [22]. The description of the various data sets has been found to be surprisingly good for all bulk observables.

For nucleus-nucleus collisions at LHC energies, one might wonder if some new features, which are not properly described by the PHSD approach within the standard settings of Ref. [9], could appear since in the initial state a color glass condensate might become important [24] or the nuclear shadowing could be different from the extrapolations given in Ref. [9], etc. To shed some light on these questions, we have tested the default PHSD version by using it to study Pb+Pb collisions at  $\sqrt{s_{NN}} = 2.76$  TeV and compared the results to data from the ALICE Collaboration [23]. In particular, we have examined the pseudo-rapidity distribution of charged particles as a function of centrality. In Fig. 1 we display the results for  $dN_c/d\eta$  at midrapidity from the default PHSD calculations in comparison to the ALICE data as a function of the number of participants  $N_{part}$  that has

been determined dynamically in the PHSD calculations. Quite acceptable agreement is seen, indicating that the bulk parton dynamics is not much different at top RHIC and LHC energies. A similar observation has also been made in Ref. [25] where the UrQMD transport approach (without explicit partonic degrees of freedom) was shown to give a reasonable reproduction of this observable as a function of centrality. Thus we continue with electromagnetic probes using the default PHSD version of Ref. [9] without readjusting any PYTHIA parameters used in the PHSD for the initial state hard scattering processes.

#### A. Partonic sources of dileptons in PHSD

The PHSD approach so far has been employed for dilepton production from  $pp$  to Au + Au collisions at SPS [6] and RHIC energies [7]. As in Refs. [6, 7] dilepton radiation from the constituents of the strongly interacting QGP proceeds via the following elementary processes: the basic Born  $q + \bar{q}$  annihilation mechanism, gluon Compton scattering ( $q + g \rightarrow \gamma^* + q$  and  $\bar{q} + g \rightarrow \gamma^* + \bar{q}$ ), and quark and anti-quark annihilation with the gluon Bremsstrahlung in the final state ( $q + \bar{q} \rightarrow g + \gamma^*$ ). In the on-shell approximation, one would use perturbative QCD cross sections for the processes listed above. However, in the strongly interacting QGP the gluon and quark propagators differ significantly from the non-interacting propagators. Accordingly, we have calculated in Refs. [26, 27] the off-shell cross sections for dilepton production in the partonic channels by off-shell partons, using the phenomenological parametrizations from the DQPM for the quark and gluon propagators and their interaction strength.

We have implemented the cross sections obtained in Refs. [26, 27] into the PHSD transport approach in the following way [7]: Whenever quark-antiquark, quark-gluon and antiquark-gluon collisions occur in the course of the Monte-Carlo simulation of the partonic phase in the PHSD, a dilepton pair can be produced according to the off-shell cross sections [27]. In addition to the virtualities of the partons involved, the latter also depends on the energy density in the local cell, where the collision takes place, as according to the DQPM it governs the widths of the quark and gluon spectral functions as well as the strong coupling.

#### B. Hadronic sources of dileptons in PHSD

In the hadronic sector, the PHSD model is equivalent to the HSD transport approach [11–13]. The implementation of the hadronic decays into dileptons ( $\pi^-$ ,  $\eta^-$ ,  $\eta'^-$ ,  $\omega^-$ ,  $\Delta^-$ ,  $a_1$ -Dalitz,  $\rho \rightarrow l^+l^-$ ,  $\omega \rightarrow l^+l^-$ , and  $\phi \rightarrow l^+l^-$ ) in HSD (and PHSD) is described in detail in Refs. [15, 28]. In contrast to the HSD approach – without explicit partonic degrees of freedom – the mesons in the PHSD are produced through the dynamical hadronization from the

partonic state. On the other hand, the subsequent interactions of the produced hadrons as well as the evolution of the hadronic ‘corona’ proceed in the same way as in the HSD.

The PHSD off-shell transport approach is particularly suitable for investigating the different scenarios for the modification of vector mesons in a hot and dense medium. As in the HSD model, the PHSD approach incorporates the *off-shell propagation* of vector mesons as described in Ref. [14]. In the off-shell transport, the hadron spectral functions change dynamically during the propagation through the medium and evolve towards the on-shell spectral functions in the vacuum. As demonstrated in Ref. [15], the off-shell dynamics is important for resonances with a rather long lifetime in the vacuum but strongly decreasing lifetime in the nuclear medium (especially  $\omega$  and  $\phi$  mesons) and also proves vital for the correct description of dilepton decays of  $\rho$  mesons with masses close to the two pion decay threshold. For a detailed description of the off-shell dynamics and the implementation of vector-meson modifications in the medium, we refer the reader to Refs. [7, 14, 15, 20, 28].

In Ref. [7], the PHSD has been extended to include hadronic sources for dilepton production from secondary multi-meson interactions through the channels  $\pi\omega \rightarrow l^+l^-$ ,  $\pi a_1 \rightarrow l^+l^-$ , and  $\rho\rho \rightarrow l^+l^-$ . These so-called ‘ $4\pi$  channels’ for dilepton production are incorporated in the PHSD on a microscopic level rather than assuming thermal dilepton production rates and a parametrization for the inverse reaction  $\mu^+ + \mu^- \rightarrow 4\pi's$  is incorporated by employing the detailed balance as in Refs. [29, 30]. By studying the electromagnetic emissivity (in the dilepton channel) of the hot hadron gas, it was shown in Refs. [2, 31] that the dominating hadronic reactions contributing to the dilepton yield at the invariant masses above the  $\phi$  peak are the two-body reactions of  $\pi + \rho$ ,  $\pi + \omega$ ,  $\rho + \rho$ , and  $\pi + a_1$ . This conclusion was supported by the subsequent study in a hadronic relativistic transport model [32]. Therefore, we implemented the above listed two-meson dilepton production channels in the PHSD approach in Ref. [7]. In addition, some higher vector mesons ( $\rho'$  etc.) were tacitly included by using phenomenological form factors that are adjusted to the experimental data. Specifically, we determined the cross sections for the mesonic interactions with dileptons in the final state using an effective Lagrangian approach following the works of Refs. [2, 32]. In order to fix the form factors in the cross sections for dilepton production by the interactions of  $\pi + \rho$ ,  $\pi + \omega$ ,  $\rho + \rho$  and  $\pi a_1$ , we used the measurements in the detailed-balance related channels:  $e^+e^- \rightarrow \pi + \rho$ ,  $e^+e^- \rightarrow \pi + \omega$ ,  $e^+e^- \rightarrow \rho + \rho$ , and  $e^+e^- \rightarrow \pi + a_1$ . Note that we fitted the form factors while taking into account the widths of the  $\rho$  and  $a_1$  mesons in the final state by convoluting the cross sections with the (vacuum) spectral functions of these mesons (using the parametrizations of the spectral functions as implemented in the PHSD). In Fig. 5 of Ref. [7] we presented the resulting cross sections that were implemented in the

PHSD. Contributions of these channels to the dilepton invariant mass spectrum in nucleus-nucleus collisions at top SPS and RHIC energies and comparisons to available data have been reported in Refs. [6, 7].

### III. THE EXTENDED STATISTICAL HADRONIZATION MODEL (SHM)

Dilepton production has also been studied in the framework of the Statistical Hadronization Model (SHM) at SPS [33] and RHIC energies [10]. Even in the absence of a dynamical evolution of the fireball, both analyses find fair agreements with measurements. In the present work, we extend the previous studies to LHC energies in order to model in detail the contribution of dileptons stemming from the so-called ‘freeze-out cocktail’. These results can then be compared with our transport simulations in order to quantify the effects from partonic degrees of freedom and the dynamical evolution of the produced hot and dense matter.

The SHM is a suitable reference model for obtaining additional dynamical information about the collisions besides the particle spectra at chemical freeze-out. A corresponding comparison for dilepton spectra from  $Au + Au$  collisions at the top RHIC energy was presented in Ref. [7]. Here we aim at a similar comparison for  $Pb + Pb$  collisions at LHC energies which requires to specify the intrinsic parameters of the statistical hadronization model. Since the central rapidity region is, to a good approximation, net charge free in heavy ion collisions at the LHC energies, we set all chemical potentials to zero in this analysis. Based on findings at SPS and RHIC, we expect the  $\gamma_S$  (strangeness suppression) factor to be close to unity in central  $Pb + Pb$  collisions at LHC energies. This was recently confirmed in Ref. [34] where measurements of ratios of hadronic rapidity densities were compared with statistical model predictions [35] evaluated with the thermal parameter  $T = 164 \text{ MeV}$  and  $\gamma_S = 1$ . All ratios of kaons and multi-strange hyperons to pions were correctly predicted, indicating that strangeness is indeed chemically equilibrated (i.e.  $\gamma_S = 1$ ) in central  $Pb + Pb$  collisions at the LHC energies. Therefore, the thermal state of the produced fireball can be specified with two free parameters: the temperature  $T$  and volume  $V$ . We do not attempt to extract the chemical freeze-out temperature from the data but use the predicted asymptotic value of  $T = 170 \text{ MeV}$  [36] instead. The overall normalization is determined from the measured transverse momentum spectra of various hadrons (see below).

The SHM - describing a static single fireball - is rather reliable in predicting the phase-space integrated relative yields of different hadrons. However, since experiments measure electrons and positrons at mid-rapidity only and above some minimum transverse momentum, we need to emulate the initial state dynamics such that the detector acceptance is correctly accounted for.

The ALICE collaboration has measured the transverse



momentum spectrum of  $\pi^-$ ,  $K^-$  and  $\bar{p}$  in the 0-5% most central Pb+Pb collisions at 2.76 TeV [34] while  $\Xi^-$  and  $\Omega^-$  spectra are measured in the 0-20% most central collisions. We can estimate the multi-strange hyperon rapidity densities in the 0-5% most central collisions with help of the combined ALICE and CMS measurement of charged hadron rapidity density as a function of centrality (see Figure 5 of [37]).

Fitting the above-mentioned charged hadron data by a second-order polynomial, we obtain the following scaling factor:

$$N_{5 \rightarrow 20\%} = \frac{dN_{ch}^{0-5\%}}{dy} / \frac{dN_{ch}^{0-20\%}}{dy} = 1612/1203 = 1.34, \quad (1)$$

by which we multiply the hyperon transverse momentum spectra in the 0-20% most central collisions in order to estimate the corresponding spectra in the 0-5% most central collisions.

We then assume that the hadron yield in  $Pb + Pb$  collisions arises as a superposition of  $N_{\text{Part}}/2$  independent nucleon-nucleon collisions and determine the average elementary volume  $V_{pp} = 2.70 \text{ fm}^3$  such that our pion yield, which scale like  $N_{\text{Part}}V_{pp}/2$ , agree with the measured pion yield in central  $Pb + Pb$  collisions. We further take  $N_{\text{Part}}=383$  independent nucleon-nucleon collisions for each 0-5% most central  $Pb + Pb$  collision.

The total mass  $M_{\text{clust}}$  of the hadron cluster in the fireball can be calculated by adding the energies of individual hadrons. From the equipartition theorem for a system in thermal equilibrium that energy is shared equally among its degrees of freedom, we can assume that the ‘‘thermal’’ momentum of the cluster  $|\vec{p}_{\text{clust}}|$  equals on average to the mass of the cluster. Since the longitudinal direction is dominantly governed by the initial state parton dynamics, we only apply this to the cluster’s transverse momentum, i.e., its average transverse momentum is  $\langle p_T^{\text{clust}} \rangle = \frac{\sqrt{2}}{\sqrt{3}} M_{\text{clust}}$ . In each event, we thus first calculate  $M_{\text{clust}}$  and sample a Gaussian distribution for the cluster’s transverse momentum such that the mean value of the Gaussian equals to  $\sqrt{2/3} M_{\text{clust}}$  while the width of the distribution is taken as  $M_{\text{clust}}/\sqrt{6}$ .

For the distribution of the longitudinal momentum of the cluster, we rely here on the simple Landau scaling, which is in fair agreement with the measurements at least up to the RHIC energies, for a discussion, see e.g. Ref. [38]. According to the Landau scaling, the width of the rapidity distribution of pions can be estimated from the simple formula

$$\sigma_y^\pi(\sqrt{s}) = \ln\left(\frac{\sqrt{s}}{2m_p}\right) \quad m_p = 0.94 \text{ GeV}, \quad (2)$$

leading to  $\sigma_y^\pi(2.76 \text{ TeV})=7.26$  which we take as the width of the clusters’ rapidity distribution in our calculations. We note that in our previous work at the RHIC energies, we have fitted the width of the clusters’ rapidity distribution with the value  $\sigma_y^\pi(200 \text{ GeV})=4.2$  which is in

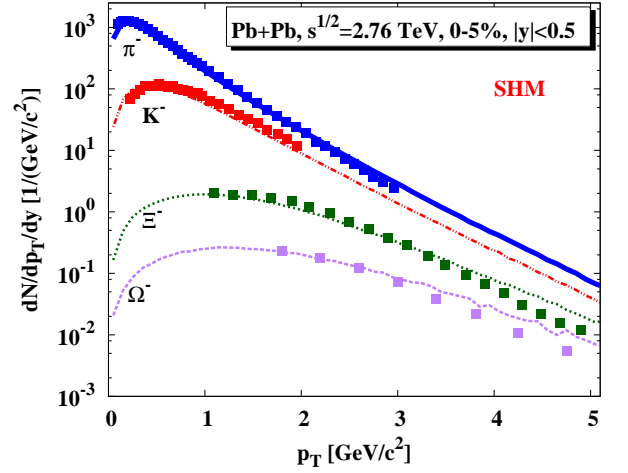


FIG. 2: (Color on-line) Transverse momentum spectra of  $\pi^-$ ,  $K^-$ ,  $\Xi^-$  and  $\Omega^-$  (squares) in  $Pb + Pb$  collisions at 2.76 TeV [34] measured by the ALICE collaboration in comparison to our statistical model calculations (lines).

fair agreement with the value  $\sigma_y^\pi(200 \text{ GeV})=4.7$  obtained from the Landau scaling. All hadrons are then boosted to the laboratory frame where the cluster moves with the momentum  $\vec{p}_{\text{clust}} = (p_T^{\text{clust}}, y_{\text{clust}}, \sqrt{p_T^{2\text{clust}} + M_{\text{clust}}^2})$ .

A comparison of our calculated transverse momentum spectra of  $\pi^-$ ,  $K^-$ ,  $\Xi^-$  and  $\Omega^-$  in central  $Pb + Pb$  collisions with ALICE measurements is presented in Figure. 2. We have omitted here the transverse momentum spectrum of  $\bar{p}$  as it is not in agreement with that measured in experiments. Nevertheless, the midrapidity data for the different hadron species is rather well described such that we can continue with the study of hadronic dilepton decays.

The form factors for dilepton decays of the light hadrons employed here are the same as in our previous study [10]. Since the low-mass dilepton spectrum is strongly dominated by hadronic decay channels, the SHM already allows us to evaluate the  $e + e^-$  pair spectrum from the different hadronic decays, i.e. the usual ‘hadronic cocktail’. On the other hand, above invariant masses of about 1 GeV the dominant hadronic channels for dileptons are the correlated and un-correlated semi-leptonic decays of open charm and open beauty mesons, whose *relative populations* are modeled within the extended SHM while the total open charm and beauty cross sections are taken from elementary p+p collisions at the same bombarding energy and scaled with the number of binary nucleon-nucleon collisions (see below).

The uncertainty in the total charm and beauty production cross sections, especially at LHC energies, is sizable. In order to estimate these cross sections, we use different (but related) models to achieve a good reproduction of the data from  $pp$  collisions at  $\sqrt{s_{\text{NN}}}=2.76 \text{ TeV}$  as described in the following Section IV. The resulting cross

sections are used to calculate the production of  $D$ - and  $B$ -mesons in  $Pb+Pb$  collisions at  $\sqrt{s_{NN}}=2.76$  TeV. Contributions from leptonic decays of these heavy mesons are then added to the dilepton spectra obtained from SHM and PHSD described in Section VI.

#### IV. OPEN CHARM AND BEAUTY

##### A. Open charm and beauty in proton-proton collisions

There are experimental indications [39, 40] that heavy flavor production might also exhibit statistical features in high energy nuclear as well as in  $e^+e^-$  collisions, at least for the relative abundances of open charm [41] and possibly also for that of open beauty mesons [42]. Since heavy-flavor production occurs early in the reactions and is not likely formed thermally, we thus extend the statistical hadronization model to include open charm and beauty mesons such that their relative yields are evaluated with the SHM (for some freeze-out temperature  $T$ ) while their total numbers are estimated from measured open and beauty production cross sections. For the  $D_s$  and  $B_s$  states, their production cross sections are multiplied by the factor  $\gamma_s^{\text{hard}}=0.3$  relative to those for nonstrange heavy mesons to take into account the strangeness suppression in hard proton-proton scattering. Furthermore, we take into account only the 6 lowest mass states of open charm mesons in the extended SHM since they already account for more than 90% of the total open charm production cross section and also not much are known about the higher mass excited states.

With the above extended SHM, we study the open charm and beauty production for the two freeze-out temperatures  $T=170$  MeV and 150 MeV while the chemical potentials are kept zero. The resulting relative normalized primary and final (after strong decays) production probabilities for the open charm states (calculated within the SHM) are given in Table I. The ratios of final open charm hadrons can then be calculated and compared with those measured by the LHCb and ALICE Collaborations in  $p+p$  collisions at  $\sqrt{s_{NN}}=7$  TeV [43–45] as shown in Table II. As one can see, all ratios are reproduced (within errors) for both temperatures of 150 and 170 MeV. We choose here, as for the light hadrons,  $T=170$  MeV as our temperature for all hadron species considered in the analysis. We note that the feed-down contribution from beauty mesons was neglected in the above analysis since this contribution is estimated to be of the order of 10% of the total charm production cross section [46].

In the above, we have taken the total open charm production cross section in  $p+p$  reactions at 7 TeV to be

$$\sigma_{cc}^{7\text{TeV}} = 6.4 \text{ mb}$$

from fitting a Gaussian to the combined measurements of ALICE and LHCb  $D$  on meson rapidity distributions. Again, the longitudinal dynamics of open heavy flavor

Hadron	primary		final state	
	T=170 MeV	T=150 MeV	T=170 MeV	T=150 MeV
$D^+$	0.186	0.200	0.273	0.286
$D^0$	0.190	0.204	0.646	0.642
$D_s$	0.0333	0.0331	0.0810	0.0751
$D^{*+}$	0.269	0.258	0	0
$D^{*0}$	0.274	0.263	0	0
$D_s^*$	0.0474	0.0420	0	0

TABLE I: Relative production probabilities of open charm mesons before (primary) and after (final) strong decays.

	LHCb [43, 44]	ALICE [45]	T=170 MeV	T=150 MeV
$\frac{D^0}{D^{*+}}$	$2.20 \pm 0.48$	2.09	2.40	2.49
$\frac{D^0}{D^+}$	$2.07 \pm 0.37$	2.08	2.37	2.25
$\frac{D^0}{D_s}$	$7.67 \pm 1.67$		7.98	8.55
$\frac{D_s^+}{D^{*+}}$	$0.94 \pm 0.22$	1.00	0.99	0.90
$\frac{D_s^+}{D^+}$	$3.48 \pm 0.93$		3.32	3.44
$\frac{D_s^+}{D_s}$	$3.70 \pm 0.84$		3.37	3.81

TABLE II: Ratios of measured [43–45] open charm yields in  $p+p$  collisions at 7 TeV compared with SHM model calculations for the temperatures  $T=170$  MeV and  $T=150$  MeV.

mesons are evaluated in the model of Ref. [10] while the transverse momentum distributions are predicted by the MC@sHQ model [47–49], explained in Section IV B. Our estimate for the total charm production cross section (6.4 mb) is comparable to the preliminary LHCb estimate of  $6.1 \pm 0.93$  mb obtained by tuning PYTHIA to the LHCb measurement and then integrating over the whole phase-space [44]. An extrapolation of the ALICE collaboration measurement at mid-rapidity to full phase-space yields, however, a cross section of  $\sigma_{cc}^{7\text{TeV}} = 8.5_{-2.4}^{+4.2}$  mb [50]. The ATLAS collaboration gives, on the other hand, for the total cross section a preliminary value of  $7.13_{-2.2}^{+4.0}$  mb [51]. The three LHC experiments agree within the uncertainties. Perturbative QCD calculations were also found to agree with the data and with our estimate for the total charm production cross section in  $p+p$  reactions at 7 TeV (see [45, 52] and references therein).

For the total charm production cross section at 2.76 TeV reads, it is estimated to be  $\sigma_{cc}^{2.76\text{TeV}} = 4.8 \pm 0.8$  mb by the ALICE Collaboration. Using the ratio of the two ALICE cross sections (at 7 TeV and at 2.76 TeV), we find that our estimate for the total cross section of charm production in  $p+p$  collisions at the lower LHC energy is

$$\sigma_{cc}^{2.76\text{TeV}} = 3.6 \text{ mb},$$

which is used in our study for heavy ion collisions at 2.76 TeV.

For the open charm decays, we have implemented in detail the form factors for each of the semi-leptonic decay channels that are included in our analysis. A discussion and presentation of relevant formulae for the open charm form factors can be found in the Appendix A. For beauty decays, no form factors were employed.

The properties of open beauty mesons are not well known experimentally and thus we use the known properties from the PDG [53] and take the missing information from model calculations. In the case of open beauty, we take into account 18 lightest states and their anti-particles. Only the lowest lying states  $B^+$ ,  $B^0$ ,  $B_s$  and  $B_s^*$  and their anti-particles decay semi-leptonically into electrons, while the excited states decay under the strong interaction into the lower mass states. It is important to take into account also the excited states in the analysis in order to properly evaluate the total beauty cross section and the relative abundances of the lowest lying  $B$  meson states. We ignore in this work the  $b$ -baryons whose production cross section is expected to be small ( $\approx 10\%$  of  $\sigma_{\bar{b}b}$ ) [53] and thus our  $\sigma_{\bar{b}b}$  refers to the total cross section for the production of open beauty *mesons*.

The properties (masses and decay channels) as well as the references to the data and models that we use for our open beauty calculations are listed in Table VI in Appendix A. In all cases we have taken a weighted average over the different estimates as input to our study, and a recent compilation for the numerical values of the open beauty masses can be found in [54].

Measurements of the total beauty cross section is not yet available at LHC energies, hence we relate it to the charm cross section and use available theoretical estimates for the ratio of these cross sections to estimate  $\sigma_{\bar{b}b}$  in p+p collisions at 2.76 TeV. We note that perturbative QCD predictions for this ratio suffer from large uncertainties [55]. Using here the same model and parameters as those applied for the calculation of the energy loss of heavy quarks in the next Section, we obtain the ratio  $\sigma_{cc}/\sigma_{\bar{b}b}=40$  in central  $Pb + Pb$  collisions at 2.76 TeV.

## B. Energy loss of D- and B-mesons in $Pb + Pb$ collisions

The total cross sections and spectra of D-mesons obtained in the previous Section from the available experimental data are for elementary p+p collisions. We are interested in the contribution of the decays of correlated and uncorrelated  $D + \bar{D}$  and  $B + \bar{B}$  pairs to the dilepton spectra in heavy ion collisions, but simple binary scaling of the spectra from p+p collisions is expected to overestimate their contributions. This is because of the neglect of the loss of correlation and the modification of the spectra of heavy hadron pairs due to the partonic energy loss [49] and hadronic rescattering [56]. To take into account the collisional and radiative energy loss of charm and beauty quarks in central Pb+Pb collisions, we use the event generator for heavy quarks and mesons of P.B. Gossiaux *et al.* – Monte Carlo for Heavy Quarks (MC@sHQ). This model – described in detail in Refs. [47–49] – assumes that in heavy-ion collisions the initial momentum distribution of charm and bottom quarks is identical to that in p+p collisions which are predicted by the FONLL PQCD calculations [57] and verified experimentally by

the STAR and PHENIX collaborations [58]. With the expansion of the produced quark-gluon plasma described by the hydrodynamic model, the interaction of heavy quarks with the plasma constituents is then calculated from the PQCD one-gluon-exchange diagrams but with a running coupling constant and an infrared regulator adjusted to reproduce the same energy loss as in the hard thermal loop calculations. Both collisional and radiative energy loss are taken into account and with the latter corrected by the Landau-Pomeranchuk-Migdal effect. This model has been shown to describe very well the nuclear modification factor  $R_{AA}$  and the elliptic flow  $v_2$  of heavy mesons (non-photonic electrons) measured at RHIC and more recently at LHC by the ALICE Collaboration [59].

Here, we employ the transverse momentum distributions of the  $D$ - and  $B$ -mesons produced in central Pb+Pb collisions as calculated in the MC@sHQ event generator as an input for our calculation of the dilepton yield by the semi-leptonic decays of  $D + \bar{D}$  and  $B + \bar{B}$  meson pairs. In particular, the decay of a single  $D$  ( $\bar{D}$ ) meson is simulated and the produced electron (positron) is combined with the positron (electron) produced in the decay of the  $\bar{D}$  ( $D$ ) meson coming from the same production vertex to form dilepton pairs from the *correlated*  $D + \bar{D}$  decays. A  $D$ -meson-decay electron is combined with a positron produced in the decay of a  $\bar{D}$ -meson coming from a (random) different production vertex but from the same event to form dilepton pairs from the *uncorrelated*  $D + \bar{D}$  decays. Furthermore, our prescription for estimating the loss of correlations due to the interactions of charm in the fireball is to multiply the yield from the correlated pairs by the suppression factor  $R_{AA}^2$ , where  $R_{AA}$  is the measured nuclear modification factor for the  $D$ -mesons. A similar procedure is used for treating the semi-lepton decays of  $B$ -mesons.

## V. CHARMONIA

### A. Charmonia in proton-proton collisions

Quarkonia are important (and experimentally clean) sources of dilepton in the high mass region and can also be used to constrain and cross-check our results regarding open charm production. Unfortunately, the SHM is not a suitable model for studying the production of the hidden charm hadrons. Therefore, we include the  $J/\psi$  and  $\psi'$  mesons in our analysis as an external input taken from the experiments, i.e. we do minimal modeling for these hadrons and take basically all necessary information from available data.

The ALICE collaboration has measured the  $J/\psi$  rapidity and transverse momentum distributions in  $p + p$  collisions at 2.76 TeV [60]. We fit a Gaussian to the measured rapidity distribution in order to extract the inclusive  $J/\psi$  production cross section of  $29 \mu b$  for this collision system as shown by the solid line in Fig. 3. According to the color evaporation model, the relative production

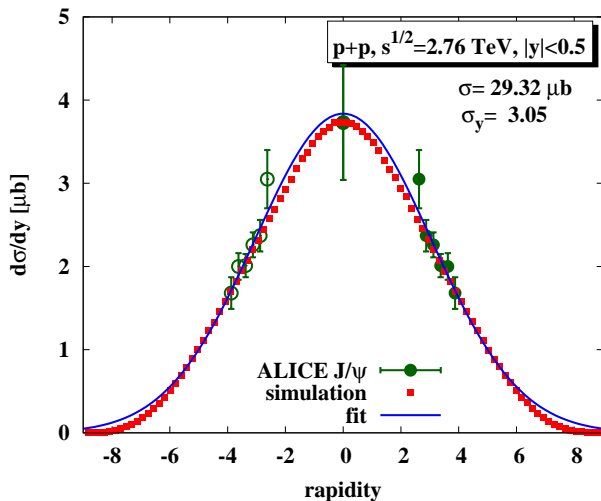


FIG. 3: (Color on-line)  $J/\psi$  rapidity distribution in  $p+p$  collisions at 2.76 TeV measured by the ALICE Collaboration [60] (full spheres) and reflection of the data (open spheres). Solid line is a Gaussian fit to the data based on a total  $J/\psi$  production cross section of  $29.3\mu\text{b}$  for this collision system. Also shown by squares is our simulated  $J/\psi$  rapidity distribution as described in the text.

probabilities of different quarkonia are beam-energy independent at ultra-relativistic energies (for a recent review, see Ref. [61]) and, once the  $J/\psi$  cross section is known, we can estimate the production cross section of  $\psi'$  in  $p + p$  collisions at 2.76 TeV with the help of the world average [62]  $\frac{\psi' \rightarrow J/\psi}{J/\psi} = 8.1\%$ .

The transverse momentum spectrum of  $J/\psi$  can also be determined from the ALICE data [60], and we use the same spectrum for  $J/\psi$  and  $\psi'$  both in  $p + p$  as well as in  $Pb + Pb$  collisions. The parameters characterizing the transverse momentum spectra of hidden and open heavy flavor hadrons are collected in Table V in Appendix B. We mention here that the details of the  $p_T$  spectrum play only a minor role in di-electron radiation from the quarkonia, while in the case of  $D$  and  $B$  meson decays the results are much more sensitive to the transverse momentum spectrum. Due to this reason, we can use the same  $p_T$  profile for quarkonia in  $p + p$  and  $A + A$  while for open heavy flavor decays the two systems have to be modeled separately.

The longitudinal momentum distributions of all heavy flavor mesons are modeled phenomenologically as explained in detail in our earlier work [10]. In the present calculations, we use the same relevant parameters (the choice of parton distributions, which determines the width of the clusters' distribution in longitudinal direction) which we have fixed at RHIC energies. Furthermore, we use the CT10 [63] parametrization for the parton distributions in all calculations. The calculated rapidity distribution of  $J/\psi$ 's within this model (with the pre-determined cross section) is compared to the ALICE data and to the Gaussian parameterizations in Fig. 3. We

find that the measured  $J/\psi$  rapidity distribution is nicely reproduced and will use the same procedure to evaluate the longitudinal momentum distributions of all heavy flavor hadrons in this work. We mention here (without explicit presentation) that the measured rapidity distributions of open charm hadrons at both mid-rapidity [45] and forward rapidities [43, 44] in  $p + p$  collisions at 7 TeV are also in good agreement with the results from this model.

## B. Nuclear modification of charmonia

To estimate the  $J/\Psi$  contribution to the dilepton spectrum in heavy ion collisions, we need information on the  $J/\psi$  nuclear modification factor in these collisions. This can be determined using the approach of Refs. [64, 65] that includes charmonium production from both initial hard nucleon-nucleon scattering and regeneration from charm and anticharm quarks in the produced QGP. For the initially produced  $J/\Psi$ , their number is proportional to the number of binary collisions between nucleons in the two colliding nuclei. Whether these  $J/\Psi$ 's can survive after the collision depends on many effects from both the initial cold nuclear matter and the final hot partonic and hadronic matters. The cold nuclear matter effects include the Cronin effect of gluon-nucleon scattering before the production of the primordial  $J/\Psi$  from the gluon-gluon fusion [66], the shadowing effect due to the modification of the gluon distribution in a heavy nucleus [67] and the nuclear absorption by the passing nucleons [68–70]. For the hot partonic and hadronic matter effects, they include the dissociation of charmonia in the QGP at temperatures higher than the dissociation temperature and the thermal decay of surviving charmonia through interactions with thermal partons in the expanding QGP. In studying these effects, medium effects on the properties of the charmonia and their dissociation cross sections are further taken into account by using the screened Cornell potential model [71] and the NLO pQCD [72]. This leads to a dissociation temperature of  $\sim 300$  MeV for  $J/\psi$  and  $\sim T_C = 175$  MeV for  $\Psi'$ , where  $T_C$  is the QCD phase transition temperature. Although the  $J/\Psi$  can survive above  $T_C$ , its thermal decay width is not small with a value of  $\sim 10$  MeV at  $T = 200$  MeV and increasing to  $\sim 100$  MeV at  $T = 280$  MeV. Because of the appreciable number of charm quarks produced in relativistic heavy-ion collisions, charmonia can also be regenerated from charm and anticharm quarks in the QGP. A rate equation is then used to include the effect of thermal dissociation and regeneration of charmonia. Since charm quarks are not expected to be completely thermalized – neither chemically nor kinetically – during the expansion of the hot dense matter, a fugacity parameter and a relaxation factor are introduced to describe their distributions. Modeling the evolution of the hot dense matter produced in relativistic heavy-ion collisions by a schematic viscous hydrodynamics [64], the average tem-



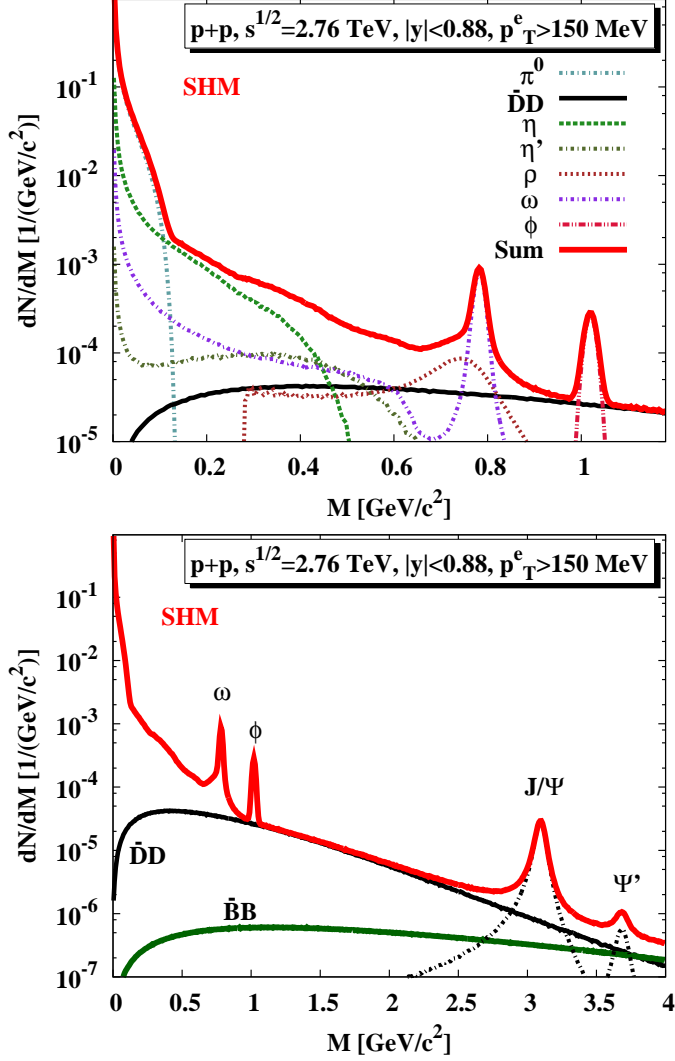


FIG. 4: (Color on-line) Dielectron invariant mass spectrum from various different sources evaluated for  $p+p$  collisions at 2.76 TeV within the SHM for the invariant mass range up to 1.2 GeV (upper window) and 4 GeV (lower window).

perature of the initially produced QGP in central Pb+Pb collisions at  $\sqrt{s_{NN}} = 2.76$  TeV is  $\sim 311$  MeV if the initial thermalization time is taken to be 1.05 fm/c. The resulting nuclear modification factors for  $J/\Psi(1S)$  and  $\Psi'(2S)$  are 0.30 and 0.39, respectively, if the shadowing effect is included. These values increase to 0.57 and 0.95, respectively, in the absence of the shadowing effect.

## VI. RESULTS

### A. The baseline: $p+p$ collisions

As a baseline for our dilepton studies, we first show in Fig. 4 the SHM results for the invariant mass spectrum of  $e^+e^-$  pairs produced in  $p+p$  collisions at  $\sqrt{s_{NN}} =$

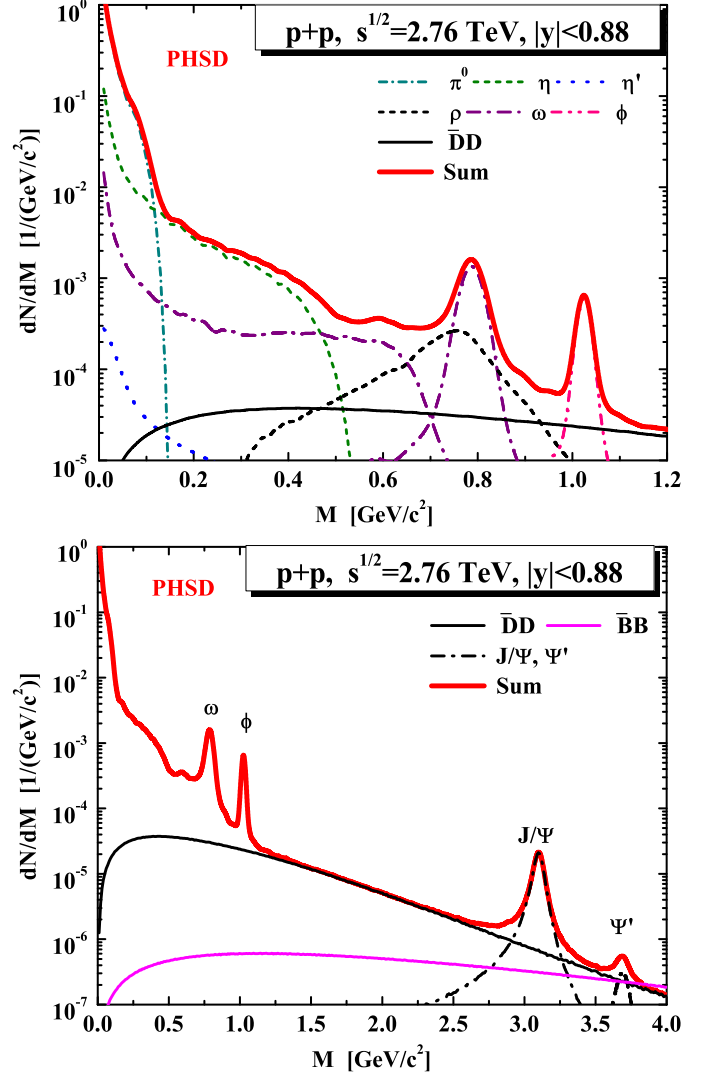


FIG. 5: (Color on-line) Same as Fig.4 from the PHSD approach.

2.76 TeV. Qualitatively, the spectra are very similar to those from the top RHIC energy of  $\sqrt{s_{NN}} = 200$  GeV [10] but enhanced by roughly a factor of 2. These results have been obtained with a transverse momentum cut of 150 MeV and a rapidity cut of  $|y_e| < 0.88$  for the single electrons, similar to the nominal acceptance cuts of the ALICE detector [73]. Also, the centrality and  $p_T$  dependent parameterizations of the ALICE detector resolution [73] have been used for determining the mass resolution. We have further included the contribution from the initial state Drell-Yan process in the collinear factorization approach of the next-to-leading-order perturbative QCD [74–76] (see also Ref. [77] for a recent discussion at LHC energies), which is expected to be compatible with the experimental data within a factor of two. We find that the Drell-Yan process contributes less than 1% in the dilepton invariant mass range considered in our studies and thus discard its contribution.

	direct	Dalitz	other
$\pi^0$	-	$\pi^0 \rightarrow \gamma e^+ e^-$	-
$\eta^0$	-	$\eta^0 \rightarrow \gamma e^+ e^-$	$\eta^0 \rightarrow \pi^+ \pi^- e^+ e^-$ (*)
$\eta'$	-	$\eta' \rightarrow \gamma e^+ e^-$	$\eta' \rightarrow \pi^+ \pi^- e^+ e^-$ (*)
$\rho^0$	$\rho^0 \rightarrow e^+ e^-$	-	-
$\omega^0$	$\omega^0 \rightarrow e^+ e^-$	$\omega^0 \rightarrow \pi^0 e^+ e^-$	-
$\phi^0$	$\phi^0 \rightarrow e^+ e^-$	$\phi^0 \rightarrow \eta e^+ e^-$ (*)	-
$J/\psi$	$J/\psi \rightarrow e^+ e^-$	$J/\psi \rightarrow \gamma e^+ e^-$	-
$\psi'$	$\psi' \rightarrow e^+ e^-$	$\psi' \rightarrow \gamma e^+ e^-$	-
$D$	-	-	$D^\pm \rightarrow e^\pm \nu_e + X$
$B$	-	-	$B^\pm \rightarrow e^\pm \nu_e + X$

TABLE III: Meson decay channels for di-electron production.

Next, we present in Fig. 5 the PHSD results for the invariant mass spectrum of  $e^+e^-$  pairs produced in  $p+p$  collisions at  $\sqrt{s_{NN}}=2.76$  TeV, employing the same transverse momentum and rapidity cuts for the single electrons, i.e.  $p_T^e > 150$  MeV and  $|y_e| < 0.88$ . We observe generally a good agreement between the two models. The minor differences in the line shapes stem from i) the production of hadrons in proton-proton collisions in the PHSD from string decays versus the thermal distribution of primary produced particles (combined with the feed-down from resonances) in the SHM and ii) the slightly different compositions of dilepton-decay channels taken into account in the SHM and the PHSD. The list of the channels for the meson decays to dileptons - contributing to the di-electron spectrum in proton-proton collisions - is presented in Table III. The (non-dominant) channels, which are taken into account in the SHM but not in the PHSD, are marked with asterisks.

### B. Results for central $Pb+Pb$ collisions at $\sqrt{s_{NN}}=2.76$ TeV

We first present the results for dilepton production from the SHM at  $\sqrt{s_{NN}}=2.76$  TeV and then compare to the spectra from the PHSD transport approach, which incorporates the same cross sections for  $c\bar{c}$  as well as  $b\bar{b}$  pair production as specified above, but also allows for an estimate of hadronic interaction channels as well as in-medium spectral functions and the radiation from the sQGP. We concentrate on most central  $Pb+Pb$  collisions, since the uncertainties in the number of participants  $N_{Part}$  are low and hadronic in-medium effects are most pronounced.

In Fig. 6 we display our results from the SHM for the dilepton low mass sector (upper window) as well as for the invariant mass range up to 4 GeV (lower window). We recall that the SHM does not include any dynamical effects and only accounts for the final hadronic 'cocktail'. The results for di-electron decays of light mesons are obtained by a scaling of  $p+p$  results with the number of participants as measured by the ALICE Collaboration [23]. The only difference between the statistical hadronization model calculations for the elementary and the heavy-ion

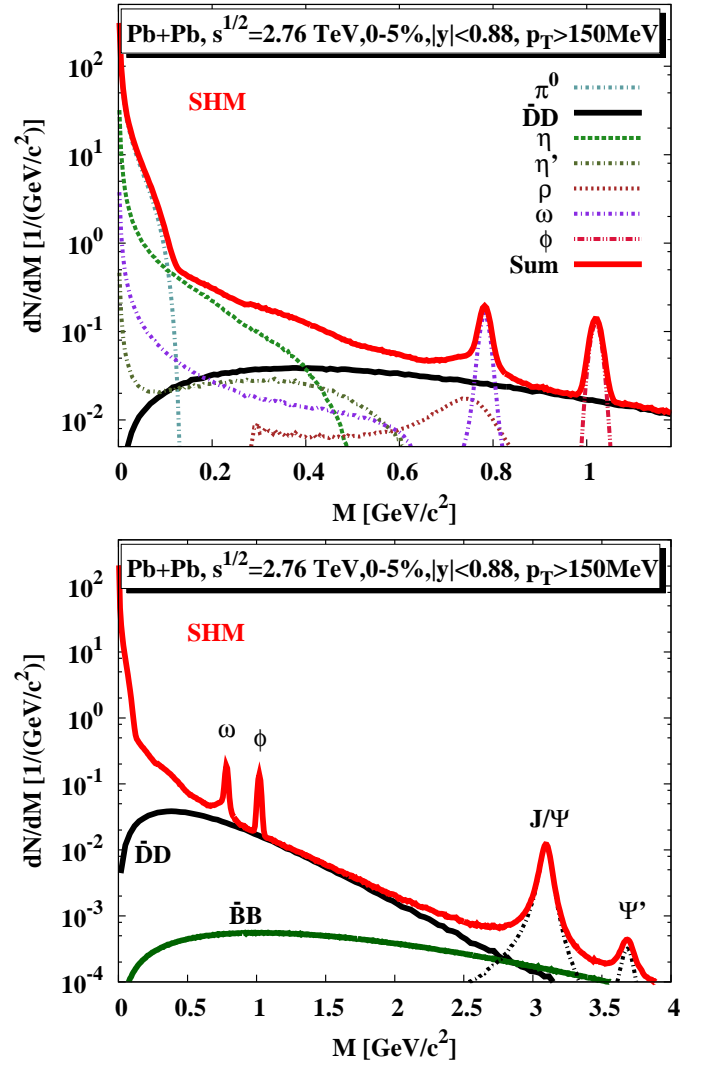


FIG. 6: (Color on-line) Dielectron invariant mass spectrum from various sources evaluated for the 0-5% most central  $Pb+Pb$  collisions at  $\sqrt{s_{NN}}=2.76$  TeV within the SHM for the dielectron invariant mass range up to 1.2 GeV (upper window) and 4 GeV (lower window). Only the un-correlated  $D$  and  $\bar{D}$  meson contributions are shown since almost all correlations are destroyed in central  $Pb+Pb$  collisions.

reactions is that  $\gamma_S=0.6$  was used for  $p+p$  collisions, while  $\gamma_S=0.95$  was used in  $Pb+Pb$  collisions, because the latter value better fits the transverse momentum spectrum of light mesons and multi-strange hyperons produced in  $Pb+Pb$  collisions at  $\sqrt{s_{NN}}=2.76$  TeV.

We point out explicitly that rescattering is fully incorporated in our calculations for the contributions from open charm and beauty decays as well as in the dilepton decays of charmonia (in Fig. 6 and in all subsequent figures in this paper). While heavy-flavor mesons are produced fully back-to-back in  $p+p$  collisions (cf. Fig. 4), we assume that these initial correlations are washed out by final-state interactions in central  $Pb+Pb$  collisions since the survival probability of the  $D$  and  $\bar{D}$  correlation

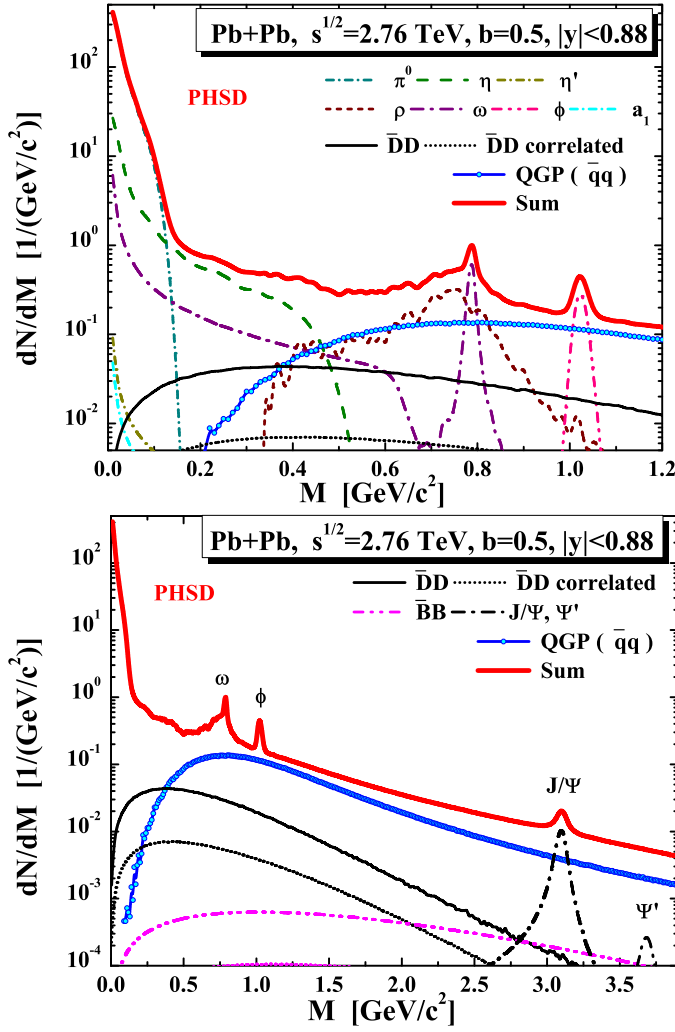


FIG. 7: (Color on-line) Same as Fig.6 from the PHSD with vacuum spectral functions for the vector mesons.

is approximately given by  $R_{AA}(D)^2$ , where  $R_{AA}$  is the  $D$ -meson nuclear modification factor. Also, the energy loss of the produced  $D$  and  $B$  mesons was taken into account, both in the correlated and uncorrelated contributions, according to the Nantes model as described in Section IV B. Additionally, the nuclear modification of charmonia was taken into account by using the predictions from Section V B.

Results from the static calculations within the SHM can be confronted with those from the dynamical transport approach PHSD that are displayed in Fig. 7. In general, the low mass spectrum from the PHSD shows a similar channel decomposition as in the SHM, while the intermediate mass region is enhanced substantially by the partonic radiation channels which are dominated by the quark-antiquark annihilation channel. We note that although the contribution of the dileptons from the correlated decays of  $D + \bar{D}$  and  $B + \bar{B}$  mesons also peaks at the intermediate mass region, its total yield is low. This is due to the fact that the (partonic) rescattering

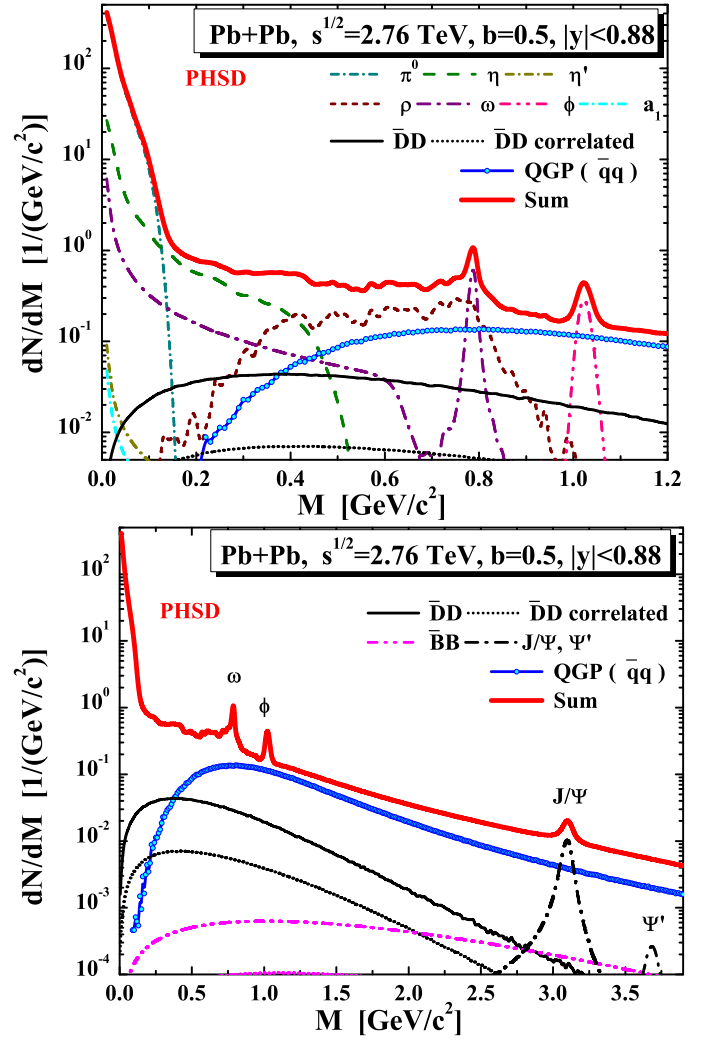


FIG. 8: (Color on-line) Upper part: Dielectron low invariant mass spectrum from various different sources evaluated for 10% central Pb+Pb collisions at  $\sqrt{s_{NN}}=2.76$  TeV within the PHSD approach including in-medium spectral functions for the vector mesons. The lower part displays our results in the mass range up to 4 GeV.

of the charm and bottom quarks in central  $Pb + Pb$  collisions practically destroys all the correlation of the initially produced heavy-quark pairs in  $p + p$  collisions. It is encouraging to see that (Fig. 7) the sQGP radiation is clearly visible in the intermediate mass region, and this provides the possibility to measure the dilepton radiation from the sQGP, making the study of its properties experimentally accessible. A similar conclusion was also made in Ref. [7] for heavy ion collisions at the top RHIC energy.

Another interesting question is the modification of the vector-meson spectral functions by hadronic in-medium effects which was found to be essential for describing the NA60 dilepton data in the low mass regime from heavy ion collisions at 158 A·GeV available from the SPS [6]. In Fig. 8 we present the dilepton invariant mass spec-

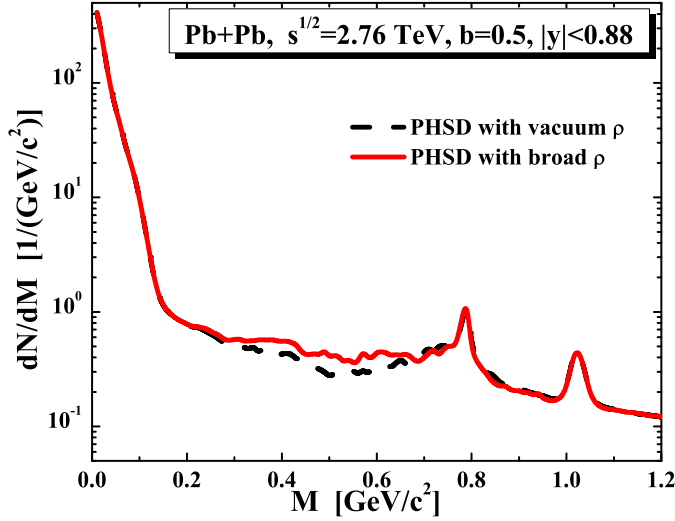


FIG. 9: (Color on-line) Dielectron low invariant mass spectrum from various different sources evaluated for most central Pb+Pb collisions at  $\sqrt{s_{NN}}=2.76$  TeV within the PHSD approach with vacuum as well as with in-medium spectral functions for the vector mesons.

trum from the PHSD in the collisional broadening scenario for the most central Pb+Pb collisions at  $\sqrt{s_{NN}}=2.76$  TeV. It is seen that the spectra in the intermediate mass region are not much affected by the medium modified vector meson spectral functions due to the dominance of partonic contributions and correlated dileptons from  $D$ -meson decays. A direct comparison of the two above calculations is displayed in Fig. 9, where we focus on the low mass sector. A moderate in-medium effect (within 20% of the total dilepton yield) in the mass window from 0.3 to 0.6 GeV due to the modification of the vector mesons can be identified.

We next study the effect of a transverse momentum cut on the channel decomposition of the dilepton spectrum. Shown in Fig. 10 are the PHSD results for the dilepton yield  $dN/dM$  in very central  $Pb+Pb$  collisions at  $\sqrt{s_{NN}}=2.76$  TeV and mid-rapidity (as in Fig. 7) but with the additional cut on the transverse momentum of single electrons of  $p_T > 1$  GeV. We find that the sQGP radiation signal in this case is even more pronounced due to the suppression of the heavy meson contribution to the dilepton yield in the intermediate masses  $M = 1 - 3$  GeV. Thus the  $p_T$  cut is beneficial to the extraction of the sQGP signal in the intermediate mass region.

On the other hand, we see in the upper part of Fig. 10 that the low-mass part of the spectrum is strongly modified by the cut: the  $\omega$  and  $\phi$  peaks become more prominent while the total yield is strongly suppressed. This loss of statistics might impair the detailed measurements of the vector meson spectral shape and of the relative meson yields. Thus we suggest that, although the cut on  $p_T$  is profitable for the measurement of the intermediate mass dileptons in order to study the sQGP radiation, the low-mass spectrum of the dileptons ( $M < 1.1$  GeV)

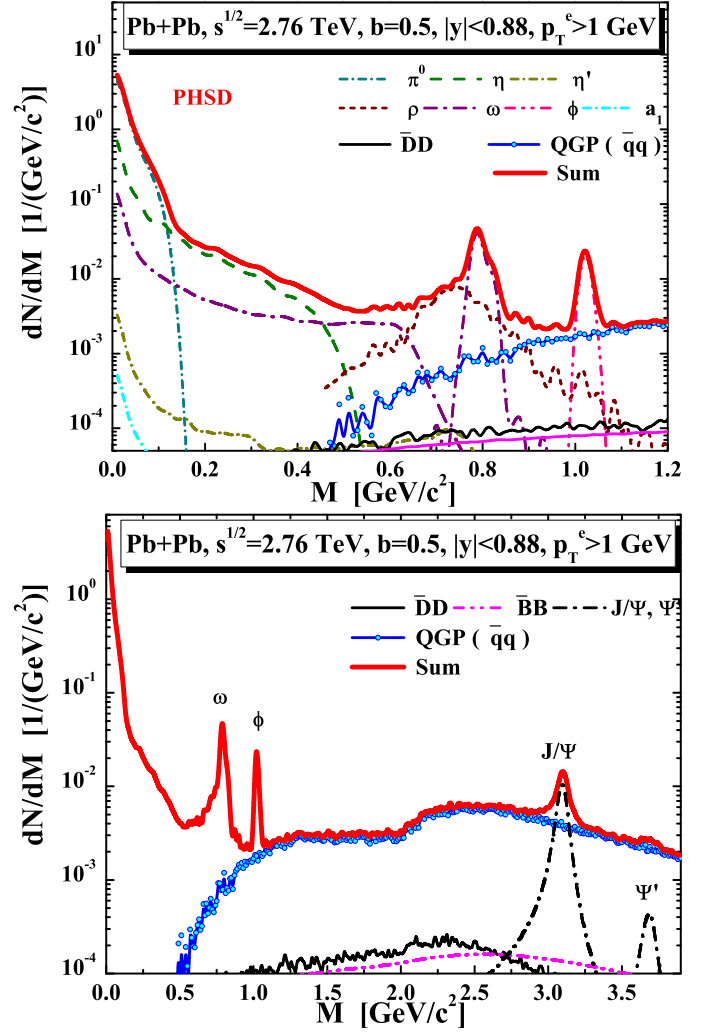


FIG. 10: (Color on-line) Upper part: Dielectron low invariant mass spectrum from various different sources evaluated for the central Pb+Pb collisions at  $\sqrt{s_{NN}}=2.76$  TeV within the PHSD approach including vacuum spectral functions for the vector mesons with the transverse momentum cut  $p_T > 1$  GeV on the single electron. The lower part displays our results in the mass range up to 4 GeV.

should better be measured down to lowest possible values of  $p_T$ .

## VII. SUMMARY

In this study, we have extended our previous investigations of dilepton production at top SPS and top RHIC energies [6, 7, 10] to  $p+p$  as well as central  $Pb+Pb$  collisions at  $\sqrt{s_{NN}}=2.76$  TeV available at the LHC by employing an extended statistical hadronization model (SHM) and the dynamical PHSD transport approach. The SHM serves to independently determine the background from the 'hadronic cocktail', while the PHSD additionally provides information on dynamical contribu-



tions to the dilepton spectrum, i.e. a low-mass enhancement due to vector meson modification by hadronic scatterings as well the contribution from partonic reactions. Both of the above dynamical effects are not visible in the final hadronic decay contributions.

In extending our previous investigations, a few new developments have been incorporated apart from a readjustment of the two SHM parameters ( $T$  and  $V$ ) to LHC energies: i) an inclusion of bottom quarks and antiquarks as well as the corresponding bottom mesons and their leptonic decay modes, ii) an appropriate model for the energy loss of open charm mesons in central  $Pb + Pb$  collisions [47–49], and iii) a dynamical approach for the charmonium suppression and recreation in the partonic and hadronic phases [64, 65] that supersedes the earlier studies within the HSD approach at lower energies [78]. With respect to the partonic channels for dilepton production in the PHSD no extensions had to be incorporated as well as with respect to the overall reaction dynamics of  $Pb + Pb$  collisions in the transport approach.

We find a reasonable agreement between the differential mass spectra of dileptons from hadronic decays calculated in the PHSD approach and the SHM model. Dynamical contributions or medium effects due to a broadened  $\rho$  spectral function is seen to give a relatively small correction in the low-mass dilepton sector from 0.3 – 0.6 GeV, since the hadronic final state interactions are less important at LHC energies. However, pronounced traces of the partonic degrees of freedom are found in the PHSD results for the intermedi-

ate mass regime, i.e. between the  $\phi$  and  $J/\Psi$  decay peaks, with the dilepton yield from the strongly interacting quark-gluon plasma (sQGP) even exceeding that from the semi-leptonic decays of open charm and bottom mesons. Additionally, we observe that a transverse momentum cut of 1 GeV/c for the leptons further suppresses the relative contribution of the heavy meson decays to the dilepton yield in the intermediate mass region, such that the sQGP radiation strongly dominates the spectrum for masses from 1 to 3 GeV, allowing for a closer look at the electromagnetic emissivity of the partonic plasma in the early phase of Pb+Pb collisions.

### Acknowledgements

The authors are grateful for the fruitful discussions with A. Andronic, J. Harris, T. Hemmick, B. Jacak, L. Ruan, J. Schukraft, I. Tserruya, A. Toia and N. Xu. J.M. and E.B. acknowledge financial support through the “HIC for FAIR” framework of the “LOEWE” program. O.L. acknowledges financial support through the Margaret-Bieber program of the Justus-Liebig-University of Giessen. The work of C.M.K. was supported by the U.S. National Science Foundation under Grants No. PHY-0758115 and No. PHY-1068572, the US Department of Energy under Contract No. DE-FG02-10ER41682, and the Welch Foundation under Grant No. A-1358.

- 
- [1] E. V. Shuryak, Phys. Lett. **B78**, 150 (1978), Sov. J. Nucl. Phys. **28** (1978) 408, Yad. Fiz. **28** (1978) 796.
  - [2] C. Song, C. M. Ko, and C. Gale, Phys. Rev. **D50**, 1827 (1994).
  - [3] G.-Q. Li and C. Gale, Phys.Rev. **C58**, 2914 (1998).
  - [4] H. van Hees and R. Rapp, Phys.Rev.Lett. **97**, 102301 (2006).
  - [5] H. van Hees and R. Rapp, Nucl.Phys. **A806**, 339 (2008).
  - [6] O. Linnyk, W. Cassing, J. Manninen, E. Bratkovskaya, and C. Ko, Phys.Rev. **C85**, 024910 (2012).
  - [7] O. Linnyk, E. L. Bratkovskaya, V. Ozvenchuk, W. Cassing, and C. M. Ko, Phys.Rev. **C84**, 054917 (2011).
  - [8] W. Cassing and E. L. Bratkovskaya, Nucl. Phys. **A 831**, 215 (2009).
  - [9] E. L. Bratkovskaya, W. Cassing, V. P. Konchakovski, and O. Linnyk, Nucl. Phys. **A856**, 162 (2011).
  - [10] J. Manninen, E. L. Bratkovskaya, W. Cassing, and O. Linnyk, Eur. Phys. J. **C71**, 1615 (2011).
  - [11] W. Cassing and E. L. Bratkovskaya, Phys. Rept. **308**, 65 (1999).
  - [12] E. L. Bratkovskaya and W. Cassing, Nucl. Phys. **A 619**, 413 (1997).
  - [13] W. Ehehalt and W. Cassing, Nucl. Phys. **A 602**, 449 (1996).
  - [14] W. Cassing and S. Juchem, Nucl. Phys. **A 665**, 377 (2000), *ibid.* **A 672**, 417 (2000).
  - [15] E. L. Bratkovskaya and W. Cassing, Nucl. Phys. **A 807**, 214 (2008).
  - [16] W. Cassing and E. L. Bratkovskaya, Phys. Rev. **C 78**, 034919 (2008).
  - [17] W. Cassing, Eur. Phys. J. ST **168**, 3 (2009).
  - [18] A. Peshier, B. Kämpfer, O. P. Pavlenko, and G. Soff, Phys. Rev. **D 54**, 2399 (1996), P. Levai and U. Heinz, Phys. Rev. **C 57**, 1879 (1998); A. Peshier, B. Kämpfer, and G. Soff, Phys. Rev. **C 61**, 045203 (2000), Phys. Rev. **D 66**, 094003 (2002); M. Bluhm *et al.*, Phys. Rev. **C 76**, 034901 (2007).
  - [19] A. Peshier and W. Cassing, Phys. Rev. Lett. **94**, 172301 (2005).
  - [20] O. Linnyk, E. Bratkovskaya, J. Manninen, and W. Cassing, J.Phys.Conf.Ser. **312**, 012010 (2011).
  - [21] E. Bratkovskaya, W. Cassing, V. Konchakovski, and O. Linnyk, Nucl.Phys. **A856**, 162 (2011).
  - [22] V. Konchakovski, E. Bratkovskaya, W. Cassing, V. Toneev, S. Voloshin, et al., Phys.Rev. **C85**, 044922 (2012).
  - [23] A. Aamodt (ALICE), Phys. Rev. Lett. **106**, 032301 (2011).
  - [24] L. McLerran, Nucl. Phys. **A 787**, 1 (2007).
  - [25] H. Petersen, **C 84**, 034912 (2011).
  - [26] O. Linnyk, S. Leupold, and U. Mosel, Phys. Rev. **D71**,

- 034009 (2005).
- [27] O. Linnyk, J. Phys. **G38**, 025105 (2011).
  - [28] E. L. Bratkovskaya, W. Cassing, and O. Linnyk, Phys. Lett. **B670**, 428 (2009).
  - [29] H. van Hees and R. Rapp, Nucl. Phys. **A 806**, 339 (2008).
  - [30] E. Santini, J. Steinheimer, M. Bleicher, and S. Schramm, Phys.Rev. **C84**, 014901 (2011).
  - [31] C. Gale and P. Lichard, Phys. Rev. **D49**, 3338 (1994).
  - [32] G.-Q. Li and C. Gale, Phys. Rev. **C58**, 2914 (1998).
  - [33] G. Agakichiev et al. (CERES), Eur. Phys. J. **C41**, 475 (2005).
  - [34] R. Preghenella (ALICE) (2012), arXiv:1203.5904.
  - [35] A. Andronic, P. Braun-Munzinger, and J. Stachel, Phys.Lett. **B673**, 142 (2009).
  - [36] J. Manninen and F. Becattini, Phys.Rev. **C78**, 054901 (2008).
  - [37] S. Chatrchyan et al. (CMS), JHEP **1108**, 141 (2011).
  - [38] M. Bleicher, J.Phys.Conf.Ser. **50**, 410 (2006).
  - [39] A. Andronic, P. Braun-Munzinger, K. Redlich, and J. Stachel, Nucl.Phys. **A789**, 334 (2007).
  - [40] S. Baumgart (2009), Ph.D. thesis, <http://drupal.star.bnl.gov/STAR/theses/phd/stephen-baumgart>.
  - [41] A. Andronic, F. Beutler, P. Braun-Munzinger, K. Redlich, and J. Stachel, Phys.Lett. **B678**, 350 (2009).
  - [42] F. Becattini, P. Castorina, J. Manninen, and H. Satz, Eur.Phys.J. **C56**, 493 (2008).
  - [43] M. Gersabeck (LHCb) (2010), 1012.3538.
  - [44] M. Schmelling and P. Spradlin (LHCb) (2010), LHCb-CONF-2010-013.
  - [45] B. Abelev et al. (ALICE), JHEP **1201**, 128 (2012).
  - [46] R. Bala (2012), arXiv:1201.0729.
  - [47] P. Gossiaux and J. Aichelin, Phys.Rev. **C78**, 014904 (2008).
  - [48] P. Gossiaux and J. Aichelin, J.Phys.G **G36**, 064028 (2009).
  - [49] P. Gossiaux, J. Aichelin, T. Gousset, and V. Guiho, J.Phys.G **G37**, 094019 (2010).
  - [50] B. Abelev (ALICE) (2012), arXiv:1205.4007.
  - [51] The ATLAS Collaboration (ATLAS) (2011), ATLAS-CONF-2011-017.
  - [52] N. Carrer and A. Dainese (2003), hep-ph/0311225.
  - [53] C. Amsler et al. (Particle Data Group), Phys.Lett. **B667**, 1 (2008).
  - [54] J. Vijande, A. Valcarce, and F. Fernandez, Phys.Rev. **D77**, 017501 (2008).
  - [55] R. Nelson, R. Vogt, C. Lourenco, and H. Wohri, Nucl.Phys. **A855**, 400 (2011).
  - [56] O. Linnyk, E. L. Bratkovskaya, and W. Cassing, Int. J. Mod. Phys. **E17**, 1367 (2008).
  - [57] M. Cacciari, P. Nason, and R. Vogt, Phys.Rev.Lett. **95**, 122001 (2005).
  - [58] L. Adamczyk et al. (STAR), Phys.Rev. **D85**, 092010 (2012), 1204.4244.
  - [59] J. Aichelin, P. Gossiaux, and T. Gousset (2012), arXiv:1201.4192.
  - [60] B. Abelev et al. (ALICE) (2012), arXiv:1203.3641.
  - [61] L. Kluberg and H. Satz (2009), arXiv:0901.3831.
  - [62] P. Faccioli, C. Lourenco, J. Seixas, and H. Woehri, JHEP **0810**, 004 (2008).
  - [63] H.-L. Lai, M. Guzzi, J. Huston, Z. Li, P. M. Nadolsky, et al., Phys.Rev. **D82**, 074024 (2010).
  - [64] T. Song, C. M. Ko, S. H. Lee, and J. Xu, Phys.Rev. **C83**, 014914 (2011).
  - [65] T. Song, K. C. Han, and C. M. Ko, Phys.Rev. **C84**, 034907 (2011).
  - [66] J. Cronin, H. J. Frisch, M. Shochet, J. Boymond, R. Mermod, et al., Phys.Rev. **D11**, 3105 (1975).
  - [67] K. Eskola, H. Paukkunen, and C. Salgado, JHEP **0904**, 065 (2009).
  - [68] B. Alessandro et al. (NA50), Phys.Lett. **B553**, 167 (2003).
  - [69] C. Lourenco, R. Vogt, and H. K. Woehri, JHEP **0902**, 014 (2009).
  - [70] R. Vogt, Phys.Rev. **C81**, 044903 (2010).
  - [71] F. Karsch, M. Mehr, and H. Satz, Z.Phys. **C37**, 617 (1988).
  - [72] Y. Park, K.-I. Kim, T. Song, S. H. Lee, and C.-Y. Wong, Phys.Rev. **C76**, 044907 (2007).
  - [73] K. Aamodt and C. Loizides (ALICE), Phys.Lett. **B696**, 30 (2011).
  - [74] G. Altarelli, R. K. Ellis, and G. Martinelli, Nucl.Phys. **B143**, 521 (1978).
  - [75] G. Altarelli, R. K. Ellis, and G. Martinelli, Nucl.Phys. **B157**, 461 (1979).
  - [76] J. Kubar-Andre and F. E. Paige, Phys.Rev. **D19**, 221 (1979).
  - [77] K. Golec-Biernat, E. Lewandowska, and A. M. Stasto, Phys.Rev. **D82**, 094010 (2010).
  - [78] O. Linnyk, E. L. Bratkovskaya, W. Cassing, and H. Stöcker, Phys. Rev. **C76**, 041901 (2007).
  - [79] D. Besson et al. (CLEO), Phys.Rev. **D80**, 032005 (2009).
  - [80] J. Link et al. (FOCUS), Phys.Lett. **B607**, 233 (2005).
  - [81] L. Widhalm et al. (Belle), Phys.Rev.Lett. **97**, 061804 (2006).
  - [82] B. Aubert et al. (BABAR), Phys.Rev. **D76**, 052005 (2007).
  - [83] D. Becirevic and A. B. Kaidalov, Phys.Lett. **B478**, 417 (2000).
  - [84] S. Fajfer and J. F. Kamenik, Phys.Rev. **D71**, 014020 (2005).
  - [85] R. Mitchell et al. (CLEO), Phys.Rev.Lett. **102**, 081801 (2009).
  - [86] J. Yelton et al. (CLEO), Phys.Rev. **D84**, 032001 (2011).
  - [87] K. Ecklund et al. (CLEO), Phys.Rev. **D80**, 052009 (2009).
  - [88] B. Bajc, S. Fajfer, and R. Oakes, Phys.Rev. **D53**, 4957 (1996).
  - [89] S. Fajfer and J. F. Kamenik, Phys.Rev. **D72**, 034029 (2005).
  - [90] L. Landsberg, Phys.Rept. **128**, 301 (1985).
  - [91] S. Godfrey and R. Kokoski, Phys.Rev. **D43**, 1679 (1991).
  - [92] D. Ebert, V. Galkin, and R. Faustov, Phys.Rev. **D57**, 5663 (1998).
  - [93] W. A. Bardeen, E. J. Eichten, and C. T. Hill, Phys.Rev. **D68**, 054024 (2003).
  - [94] P. Colangelo, F. De Fazio, and R. Ferrandes, Nucl.Phys.Proc.Suppl. **163**, 177 (2007).
  - [95] N. Isgur and M. B. Wise, Phys.Rev.Lett. **66**, 1130 (1991).
  - [96] A. M. Green, J. Koponen, C. McNeile, C. Michael, and G. Thompson (UKQCD), Phys.Rev. **D69**, 094505 (2004).
  - [97] I. V. Gorelov (CDF) (2006), hep-ex/0610080.

### Appendix A: $D$ meson form factors

The form factors for  $D^0 \rightarrow K^- e^+ \nu_e$  decays have been measured by CLEO [79], FOCUS [80], BELLE [81] and BaBar [82] Collaborations. These can be conveniently parametrized in the modified pole ansatz [83]

$$f_+(q^2) = \frac{f_+(0)}{(1 - \frac{q^2}{m_{D_s^*}^2})(1 - \alpha \frac{q^2}{m_{D^*}^2})}. \quad (\text{A1})$$

We take a weighted average  $\alpha=0.35$  of the measured [79–82]  $\alpha$  and  $m_{D_s^*}=2.112$  GeV as our input for the calculations and use the same parameters for the corresponding  $D^\pm$  decays.

The measured [79–81] form factors for  $D \rightarrow \pi l \nu_e$  decays can be parametrized in the simple pole approximation

$$f_+(q^2) = \frac{f_+(0)}{(1 - \frac{q^2}{m_{pole}^2})}, \quad (\text{A2})$$

in which we take a weighted average  $m_{pole}=1.92$  GeV as input for our calculations.

The other  $D \rightarrow P e \nu_e$  form factors have not been measured yet and thus we will rely on theoretical modeling here. We use the formalism [84] introduced by Fajfer and Kamenik in which the form factor for the decay of a  $D$  meson ( $H$ ) has the same form as Eq. (A1) but the parameters of the distribution are fixed to the masses of the known (nearest) resonances. Explicitly, it is given by

$$f_+(q^2) = \frac{f_+(0)}{(1 - \frac{q^2}{m_H^2})(1 - \alpha \frac{q^2}{m_{H^*}^2})}, \quad (\text{A3})$$

where  $\alpha = m_{H^*}^2/m_{H^*}^2$ . The nearest pole masses  $m_{H^*}$  and  $m_{H^*}$  that fix the value of the  $\alpha$  parameter are process dependent and are listed in the Table I of [84]. The predictions [84] of the Fajfer-Kamenik model for the semi-leptonic branching fractions  $D^+ \rightarrow \{\eta', \eta\} e^+ \nu_e$  were recently confirmed by the measurements [85, 86] of the CLEO Collaboration. With the help of the form factors, the  $q^2$  distribution of the  $D \rightarrow \text{pseudo-scalar} + e + \nu_e$  can be calculated from

$$\frac{d\Gamma}{dq^2} \sim |p_X(q^2)|^3 |f_+(q^2)|^2, \quad (\text{A4})$$

where  $X = \{K, \pi, \eta, \eta', f_0\}$ . The parameters we have used for the  $D \rightarrow P e \nu_e$  transitions are listed in Table IV.

The  $D_{(s)} \rightarrow V e \nu$  with  $V$  denoting a vector meson ( $K^*$  or  $\phi$ ) decays can be parametrized with the help of three form factors [88, 89]

$$\begin{aligned} V(q^2) &= \frac{V(0)}{(1-x)(1-ax)}, \\ A_1(q^2) &= \frac{A_1(0)}{1-b'x}, \quad A_2(q^2) = \frac{A_2(0)}{1-b'x} \end{aligned} \quad (\text{A5})$$

channel	$m_{pole}$ [GeV]	$\alpha$	references
$D \rightarrow \pi e \nu_e$	1.92	0	[79–81]
$D \rightarrow K e \nu_e$	2.112	0.385	[79–82]
$D \rightarrow \eta e \nu_e$	2.010	0.74	[84]
$D \rightarrow \eta' e \nu_e$	2.010	0.74	[84]
$D_s \rightarrow \eta e \nu_e$	2.112	0.75	[84]
$D_s \rightarrow \eta' e \nu_e$	2.112	0.75	[84]
$D_s \rightarrow K e \nu_e$	2.010	0.74	[84]
$D_s \rightarrow f_0(980) e \nu_e$	1.7	0	[87]

TABLE IV: List of parameters characterizing the  $D \rightarrow P e \nu_e$  transitions.

in the helicity amplitude formalism. In the above,  $x = q^2/m_{pole}^2$  with  $m_{pole}$  being the (process dependent) pole meson mass and the free parameters of the model ( $V(0)$ ,  $A_1(0)$ ,  $A_2(0)$ ,  $a$  and  $b$ ) were determined in [89] (see Table I of [89] for the list of  $m_{pole}$  and Table II for the values of the fit parameters), and we use these parameters in our calculations.

The  $q$ -distribution of the total decay rate is evaluated with

$$\begin{aligned} \frac{d\Gamma}{dy} &= \frac{d(\Gamma_+ + \Gamma_- + \Gamma_0)}{dy} \\ &\sim y |p_{\vec{V}}(y)| (|H_+(y)|^2 + |H_-(y)|^2 + |H_0(y)|^2) \end{aligned} \quad (\text{A6})$$

where  $y = q^2/m_H^2$  and

$$|p_{\vec{V}}(y)|^2 = \frac{(m_H^2(1-y) + m_V^2)^2}{4m_H^2} - m_V^2 \quad (\text{A7})$$

is the three momentum of the vector meson in the rest frame of the  $D$  meson, and the helicity amplitudes read

$$\begin{aligned} H_\pm(y) &= (m_H + m_V) A_1(m_H^2 y) \mp \frac{2m_H |p_{\vec{V}}(y)|}{m_H + m_V} V(m_H^2 y), \\ H_0(y) &= \frac{m_H + m_V}{2m_H m_V \sqrt{y}} (m_H^2(1-y) - m_V^2) A_1(m_H^2 y), \\ &\quad - \frac{2m_H |p_{\vec{V}}(y)|}{m_V(m_H + m_V) \sqrt{y}} A_2(m_H^2 y). \end{aligned} \quad (\text{A8})$$

We have implemented in detail the form factors for each and every of the known open charm semi-leptonic decay channels. The only decay channel that is considered isotropic in the momentum space is the  $D \rightarrow \rho^0 e \nu_e$ . Due to the large width of the  $\rho^0$ , above formalism is not applicable for this channel. One could implement the ISGW2 parametrization, but this channel contributes 3% of the total semi-leptonic decay width for  $D^0$  and even less for the  $D^+$ . Omission of this form factor should not cause much effect.

### Appendix B: Characteristics of the transverse momentum spectra

We do not calculate the transverse momentum spectrum of heavy hadrons within the SHM but fit a power-

Hadron	system	Ref.	B [GeV]	n	$p_T$ [GeV]
$J/\psi$	p+p 2.76 TeV	[60]	4.53	4.61	[0:8]
$D$	p+p 2.76 TeV	[47–49]	2.37	3.09	[0:10]
$B$	p+p 2.76 TeV	[47–49]	6.38	3.10	[0:10]
$D$	Pb+Pb 2.76 TeV	[47–49]	2.10	3.78	[0:10]
$B$	Pb+Pb 2.76 TeV	[47–49]	4.19	3.24	[0:10]

TABLE V: Parameters characterizing the heavy flavor transverse momentum spectra around mid-rapidity in  $p+p$  and  $Pb+Pb$  collisions at 2.76 TeV.

Hadron	mass	relevant branching fractions
$B^+$	[53]	$e^+\nu_e X_c$ 10.2%
$B^0$	[53]	$e^+\nu_e X_c$ 10.1%
$B^{*+}$	[53]	$B^\pm\gamma$ 99% $B^\pm e^+e^-$ 0.5% [90]
$B^{*0}$	[53]	$B^0\gamma$ 99% $B^0 e^+e^-$ 0.5% [90]
$B_0^+$	[91–94]	$B\pi$
$B_0^0$	[91–94]	$B\pi$
$B_1^+$	[53]	$B^*\pi$ [95]
$B_1^0$	[53]	$B^*\pi$ [95]
$B_1^{*+}$	[91–94]	$B^*\pi$ [95]
$B_1^{*0}$	[91–94]	$B^*\pi$ [95]
$B_2^{*+}$	[53]	$B\pi$ 40% $B^*\pi$ 60% [95]
$B_2^{*0}$	[53]	$B\pi$ 40% $B^*\pi$ 60% [95]
$B_s$	[53]	charm
$B_s^*$	[53]	$B_s^0\gamma$
$B_{s0}$	[91–94, 96]	$BK$ [97]
$B_{s1}$	[53]	$B^*K$ [97]
$B_{s1}^*$	[91–94, 96]	$B^*K$ [97]
$B_{s2}^*$	[53]	$B\pi$ 60% $B^*\pi$ 40%

TABLE VI: References to the works from which we have taken the  $B$  meson masses and relevant branching ratios. Unless explicitly stated otherwise, the branching fractions to the listed channels are 100%

law function to the available experimental data ( $J/\psi$ ) and theory calculations ( $D$  and  $B$  mesons) and use these parameterizations as our input for the simulations. We list here all the relevant parameters related to transverse momentum spectra of various hadrons. Explicitly,

$$\frac{d^2N}{dp_T dy} = C(y) \frac{p_T}{\left(1 + \frac{p_T^2}{B^2}\right)^n}, \quad (\text{B1})$$

where  $C(y)$  is some rapidity dependent normalization factor and the parameters  $B$  and  $n$  are listed in Table V along with the references to the input data.

We use the same  $p_T$  spectrum for  $\psi'$  as that for  $J/\psi$ . In contrast to the dilepton emission from  $D$  and  $B$  mesons, our results do not depend strongly on the details of the  $J/\psi$  transverse momentum spectrum and hence we use the same parameters for  $Pb+Pb$  collisions as in  $p+p$  collisions.

### Appendix C: Properties of open beauty mesons

Properties of open beauty mesons are given in Table VI.